Morphology and hole transport of butadiene derivative

Toshio Enokida[a)]
Graduate School of Science and Technology, Chiba University, 1-33 Yayoi-cho, Chiba-shi, Chiba 260, Japan

Ryo Hirohashi
Faculty of Engineering, Chiba University, 1-33 Yayoi-cho, Chiba-shi, Chiba 260, Japan

(Received 28 May 1991; accepted for publication 28 August 1991)

Morphology and hole-carrier mobilities of 1,1-bis(*p*-diethyl-aminophenyl)-4, 4-diphenyl-1, 3-butadiene (DEAB) derivative have been investigated. Annealing on a DEAB film and the temperature of glass transition, crystallization and the melting point on this amorphous film were measured by a differential scanning calorimeter and their polymorphic states discussed. Hole-carrier mobilities in excess of 10^{-3} ($cm^2/V\,s$) have been observed at room temperature. The electric field and temperature dependences of the hole mobility can be described as $\exp(\beta E^{1/2})$ and $\exp(T_0/T)^2$ and are discussed according to Arrhenius, Poole–Frenkel formulations and non-Arrhenius type of temperature dependence assuming Gaussian distribution of the hopping sites.

I. INTRODUCTION

The carrier transport of conductive polymer systems and molecularly doped polymers has been investigated in the study of organic photoreceptors for electrophotography.[1–5] The time-of-flight (TOF) technique has been used to measure the charge-carrier mobilities as a function of their electric field, temperature, dopant concentration, and dopant molecule dependences. Transient photocurrents for measuring the flight time of charge carriers in photoconductive films were analyzed according to the theory in logarithmic units of current versus time proposed by Scher and Montroll.[1] In particular, the shape of the transient photocurrent, and film thickness, concentration, electric field and temperature dependences of the transit time (t_T) have been studied to reveal the details of the transient mechanism.

In recent years, molecularly doped polymers have been widely used, and the charge transport of these materials has been investigated.[3–5] The materials are usually prepared as solid solutions which contain a strong electron donor or acceptor in a polymer such as bisphenol-*A*-polycarbonate. The mobilities are typically 10^{-3}–10^{-9} $cm^2/V\cdot s$, therefore a hopping theory has been shown to satisfactorily explain the charge transport instead of the band transport. Another model of charge transport, which is based on disorder in organic molecular solids, has been proposed by Bässler *et al.*[6,7] This model shows the disorder to split the transport bands, characterized by non-Arrhenius-type temperature dependence of the diffusion. Thus the carrier transport is governed by traps outside the distribution of the hopping sites.

This paper describes the polymorphic states of the crystal powder and the cast film of 1,1-bis(*p*-diethyl-aminophenyl)-4, 4-di-phenyl-1, 3-butadiene (DEAB) derivative.[8,9] Thermograms of the crystal powder and the cast film were analyzed by a differential scanning calorimeter (DSC) and an annealing technique. In addition, the electric field and temperature dependences of hole carrier mobility on the DEAB derivative were investigated by Arrhenius and non-Arrhenius systems. It is well known that the mobilities of the polymer can influence the photogeneration and charge transport of the molecularly doped polymer,[3] therefore the DEAB amorphous film without the addition of polymers was used in this study.

II. EXPERIMENT

A. Materials and analytical measurements

The measured samples in this study are the 1,1-bis(*p*-diethylaminophenyl)-4, 4-diphenyl-1, 3-butadiene (DEAB) derivative. The structure of this derivative is shown in Fig. 1. The x-ray diffraction (XRD) patterns were recorded on a Rigaku RU-200 equipped with a Cu$K\alpha$ monochromatic radiation. The coated films were annealed by a heating oven at various temperatures for 10 min each. IR spectra were measured for samples dispersed on a KBr pellet on a Japan Spectroscopic Co. infrared spectrophotometer IR-700 with a grating monochrometer. The absorption spectrum was measured on a Japan Spectroscopic Co. UV-2100 spectrophotometer with the DEAB derivative in chloroform. The fluorescence spectrum was measured on a Shimadzu RF-510 spectrofluorophotometer. The solution used was chloroform, and the concentration of the solution was 5×10^{-4} (mol/ℓ). The excited wavelength in this fluorescence was measured at 456 nm. Thermograms were recorded on a MAC Science DSC-3100. Calorimetric quantities were calculated from areas under the transition peaks. The calorimeter was calibrated using the heat of fusion of aluminum oxide (α-Al_2O_3), and the heating rate was kept constant at 5 K/min. Annealing of films was done in a furnace at pertinent temperature from 313 to 413 K for 30 min.

[a)]On leave from Electronic Materials Division, Toyo Ink Mfg. Co., Ltd., 1 Sakae, Kawagoe-shi, Saitama 350, Japan.

 0021-8979/91/116908-07$03.00

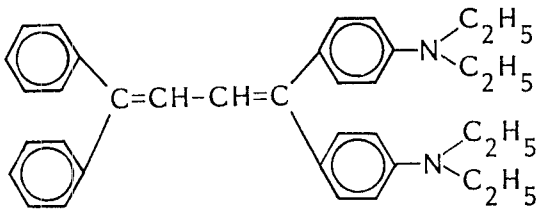

FIG. 1. Structure of DEAB derivative.

B. Time-of-flight technique

The samples measured in this study are solid films of the DEAB derivative. This sample was solvent coated onto NESA glass to a thickness of 15 ± 1 μm and was dried slightly at 298 K for a few days. The solvent employed was chloroform in this work. An opposite gold electrode of film on NESA glass was deposited on the surface of the film. The charge generation materials were not used, because this DEAB itself can generate hole carriers.

The hole-carrier drift mobilities were measured by the usual TOF technique used by the apparatus as shown in Fig. 2. A pulse of 337-nm N_2 laser with 5-ns duration was used to generate free carrier in a DEAB layer through the NESA glass. The sample was used as a condensor in a resistor-capacitor (RC) circuit, and the RC values were determined to be less than the transit time. The voltages were applied to the sample immediately before the pulse irradiation. The current transients were collected by a Kawasaki Electronica M-100E interfaced to a Iwatsu Electric Co., Ltd. Synchroscope SS-5711 and a computer. All transit times were measured on current-versus-time scales, and were determined to be the shoulders which indicated no dispersive transport of the charge packet through the films. The shoulders suggested t_T, and these values were calculated with the following equation

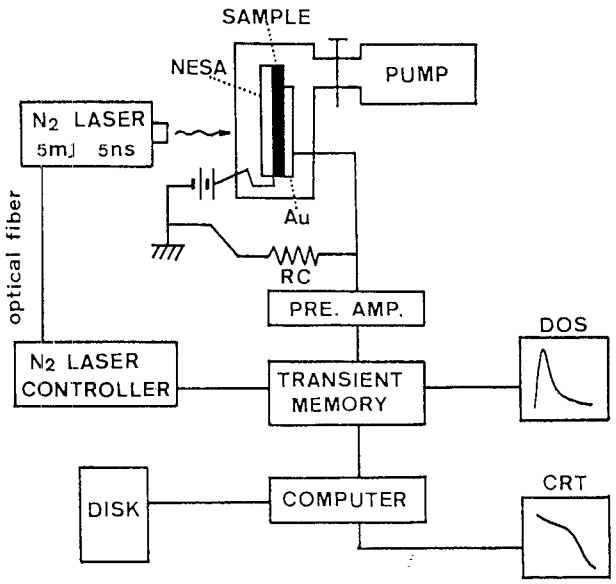

FIG. 2. Schematic diagram of the carrier drift mobility apparatus.

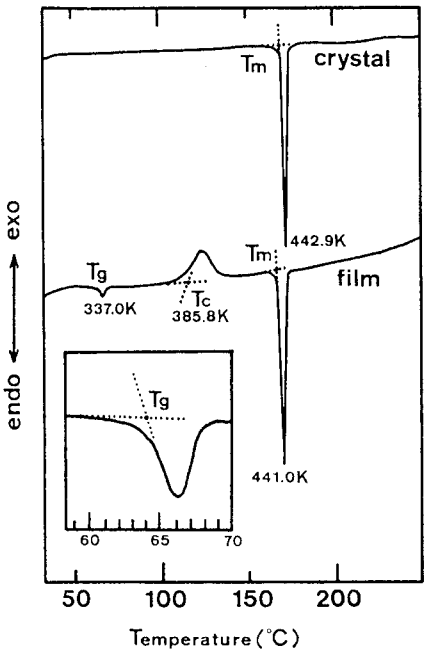

FIG. 3. DSC thermograms of DEAB derivative. Heating rate is 5 K/min. (a) crystal, (b) casted film.

$$\mu = L^2/V \cdot t_T, \tag{1}$$

where L is the thickness of the sample films, μ is the mobility, and V is the applied voltage. The light intensity and the thickness of the sample films did not depend on the mobilities in this paper.

III. RESULTS AND DISCUSSION

A. DSC analysis

DSC analysis was carried out on both the crystal powder and the casted film of the DEAB derivative. The results are shown in Fig. 3 and Table I. When the crystal powder of the DEAB derivative is heated from room temperature, an endothermic peak due to the melting is observed at 442.9 K. The enthalpy change (ΔH) for the melting is 24.3 kJ/mol. When the cast amorphous film is heated from room temperature, an endothermic peak is observed at 337.0 K, which is around the glass transition temperature. Then a broad exothermic peak due to crystallization is observed at 385.8 K, followed by an endothermic peak due to the melting at 441.0 K. The ΔHs of the glass state change, the crystallization, and the melting are 1.27, 15.2,

TABLE I. The endothermic and exothermic peaks and enthalpy changes (ΔH) of DSC curves of DEAB derivatives. T_g = glass transition temperature, T_c = crystallization temperature, and T_m = melting temperature.

	T_g	T_c	T_m
Crystal	-	-	442.9 K 24.3 kJ/mol
Casting film	337.0 K 1.27 kJ/mol	385.8 K 15.2 kJ/mol	441.0 K 19.4 kJ/mol

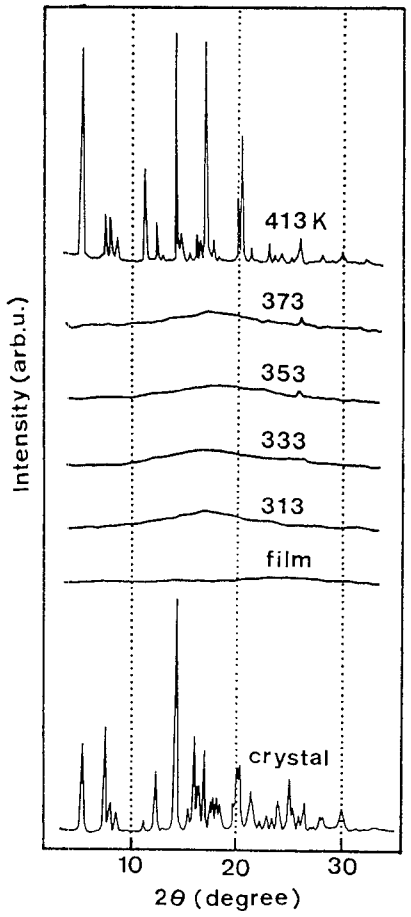

FIG. 4. XRD patterns of DEAB derivative. (a) crystal, (b) casted film.

and 19.4 kJ/mol, respectively. As shown in Fig. 3, polymorphic differences between the crystal powder and the cast film can be seen; therefore, the DEAB films were annealed and their XRD patterns measured.

B. Annealing and x-ray diffractometry

In order to analyze the behavior of the crystal state, these films were annealed, and their XRD patterns were measured. The XRD patterns indicate what lattice defects or crystal transformations are formed, which depend upon how the films were prepared. Figure 4 and Table II show

TABLE II. Main peak lines of XRD patterns of DEAB derivatives.

2θ (°)	I/I_0	d (Å)
5.7	39	15.5
7.8	45	11.3
12.5	28	7.1
14.5	100	6.1
16.4	42	5.4
16.7	21	5.3
17.2	36	5.1
20.3	28	4.37
20.6	31	4.31
21.6	20	4.11
25.2	23	3.53

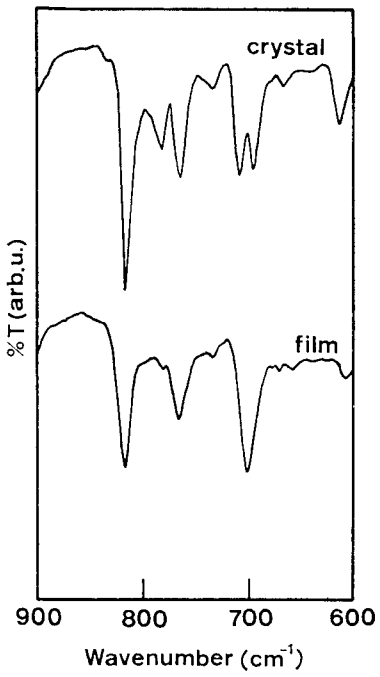

FIG. 5. IR spectra of DEAB derivatives. (a) crystal, (b) casted film.

the XRD patterns and diffraction lines of the main peaks on the DEAB derivative and its polymorphic change by an annealing method. The crystal powder shows several peaks; on the contrary, the casted film shows an amorphous state. The diffraction intensity of the crystal powder was intense; that is, especially a peak at $2\theta = 14.5°$ showed strong intensity. Using the Bragg equation, $\lambda = 2d \cdot \sin\theta$, to associate a spatial repeat period with $2\theta = 14.5°$ the peak yields $d = 6.1$ Å. The assignment of this distance (6.1 Å) cannot be obtained since no single crystal is prepared for crystal structure observation, however, it is presumed that hole drift carriers in the DEAB film can easily transfer by hopping conduction within this distance, because the intermolecular distance of 100% DEAB for carrier hopping can be estimated to be approximately 9 Å by the concentration dependence of the mobility.[10] The films annealed under 373 K have no definite peaks, indicating that the molecules of the butadiene derivative are not stacked regularly. On the contrary, after annealing at 413 K, which suggests the temperature between crystallization and melting in the aforesaid DSC result, intense and numerous peaks appeared at positions similar to those of the crystal powder of DEAB derivative. This result indicates that the amorphous film can be recrystallized, and the crystallization of the amorphous film is governed by thermal energy.

C. IR spectra

The IR spectra of the crystal powder and the cast film of the DEAB derivative are shown in Fig. 5. Slight differences can be seen in the ranges of 700–800 cm^{-1}. These frequencies are assigned to the out-of-place C—H bending vibrations of the peripheral benzene rings of the DEAB derivative. In the case of casted amorphous film, the two broad absorption lines at 700 and 763 cm^{-1} can be found

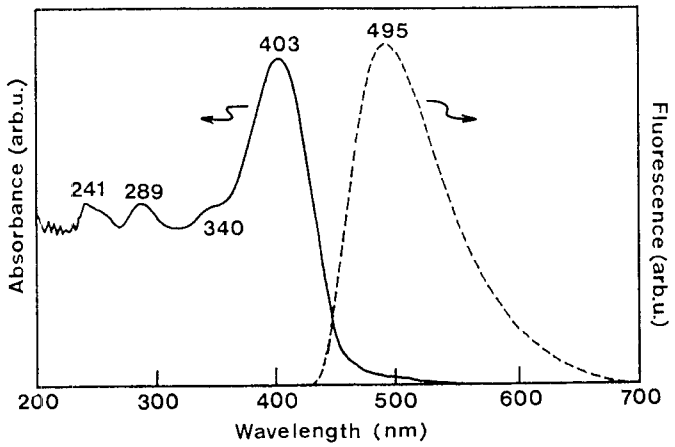

FIG. 6. Vis/UV and fluorescence spectra of a solution of DEAB derivative. The solution used was chloroform. Both spectra were measured on the same concentration of 5×10^{-4} (mol/ℓ). The excited wavelength for fluorescence spectra was measured at 456 nm.

at 700–800 cm^{-1}. On the other hand, an absorption line of the crystal powder at approximately 700 cm^{-1} is split into two lines of 692 and 706 cm^{-1}, and the line at 780 cm^{-1} is found to be apparent. Since the molecules in the amorphous film are not configurationally limited and their intermolecular interaction will become weaker than the crystal powder film, therefore, their vibrations may counteract each other, and no apparent absorption can be seen at 780 cm^{-1}.

D. Absorption and fluorescence spectra

Fluorescence spectroscopy is a method for investigating the relaxed excited states. Figure 6 shows the absorption and fluorescence spectra of the DEAB derivative in chloroform. The maximum peak of the absorption spectrum appears at 403 nm, while the fluorescence peak occurs at 495 nm. Both spectra are mirror images of each other. This DEAB derivative shows a large fluorescence peak due to the characteristics of excimers from excited states to ground states, which indicates the excellent exciton-generation ability. When we think of a potential energy diagram for a pair of molecules, molecular approach increases the resonance energy, and the fluorescence spectrum can be measured over a longer wavelength region than the absorption spectrum.

E. Electric field and temperature dependences of hole mobility followed by Poole–Frenkel and Arrhenius mechanism

Figure 7 shows a typical photocurrent time-evolution curve of a DEAB film (16-μm thick) which is observed for holes on a field of 10^4 V/cm at 298 K. The t_T was determined by the intersection of the tangents to the current before and after the sharp decrease in current. Therefore, the mobilities were calculated from the t_T in this work. The transient photocurrent showed a relatively obvious t_T on a linear current-time plot, however, the t_T was measured by the log i-log t plot in order to obtain accurate mobilities. In

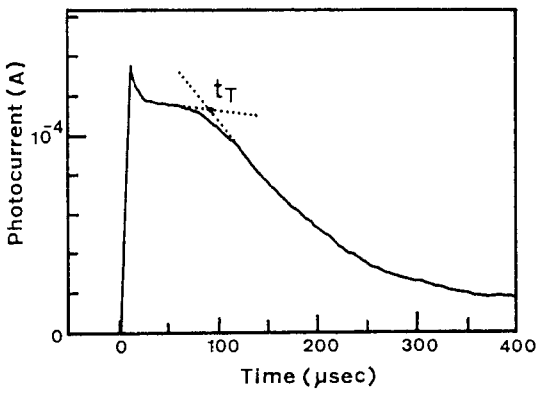

FIG. 7. A typical photocurrent time-evolution pulse of a 16-μm sample measured at an electric field of 10^4 V/cm. The transit time is 101 μs, corresponding to a mobility of 1.22×10^{-3} $cm^2/V\cdot s$ at 294 K.

this measurement, the photocurrent was monitored over 10^{-4} A, which was a very large current compared with other photoconductive derivatives. The large fluorescence spectrum of this derivative can be seen in Fig. 6, and the photocurrent was also very large. These high mobilities of more than 10^{-3} $cm^2/V\cdot s$ were observed at room temperature.

Figure 8 shows the square root of the electric field ($E^{1/2}$) (where E is V/L) dependence of the hole mobilities. The mobilities exhibit a linear relationship, and the small field dependence of the mobilities implies that this derivative is relatively free from deep structural traps, that is, the carriers can escape from a charged trapping center into the conduction band under the influence of the applied field. The DEAB has many phenyl group and double bonded carbons in the butadiene skelton for large resonances in the molecule. Therefore, the intra- and intermolecular transfer of carriers is rapid, and effective hopping distances would be shorter than in other charge transport materials such as hydrazone derivatives.[5] From many experimental observations, $E^{1/2}$ was consistent with the data and gave linear plots of log μ vs $E^{1/2}$. The $E^{1/2}$ dependence is explained by the Poole–Frenkel effect. This Poole–Frenkel model indicates the lowering of a Coulomb barrier in the presence of the electric field. The molecules giving rise to weakly field-dependent mobilities can be character-

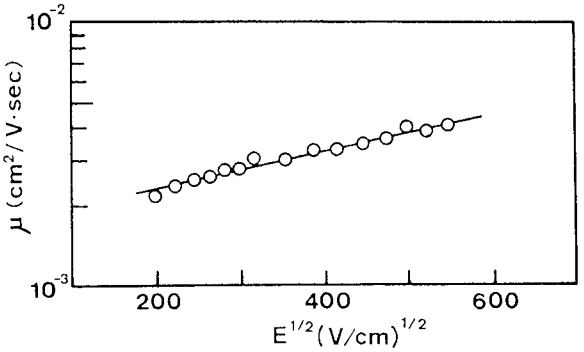

FIG. 8. The logarithm of the mobility vs $E^{1/2}$.

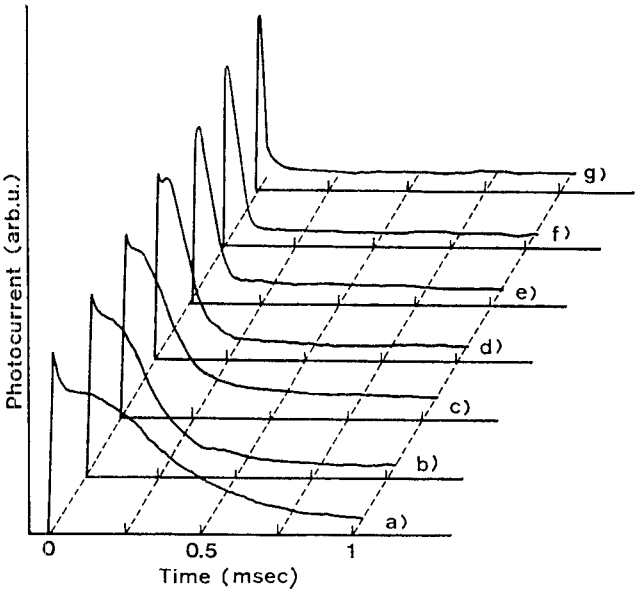

FIG. 9. Pulse shapes at various temperatures. (a) 283.5 K, (b) 293.6 K, (c) 297.5 K, (d) 305.5 K, (e) 313.3 K, (f) 325.0 K, (g) 335.6 K; $E = 10^4$ V/cm.

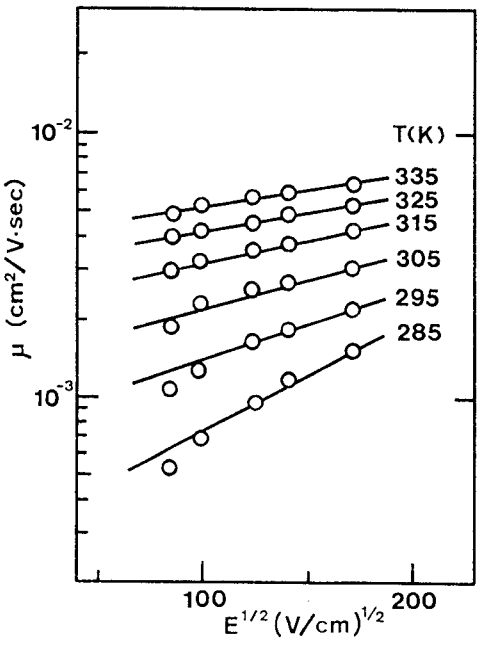

FIG. 10. The logarithm of the mobility vs $E^{1/2}$ at various temperature.

ized by low T_0 (or high T_{eff}).[11] Thus, T_0 is an important parameter to study the transport mechanism of molecular-doped systems as described below. The average distances between DEAB molecules is calculated from the following formula

$$\rho = [M/(A \cdot d)]^{1/3}, \tag{2}$$

where ρ is the average distance, M is the molecular weight of DEAB derivative, A is Avogadro's number, and d is the density ($d = 1.21$). The ρ of this amorphous film containing DEAB derivative is approximately 9 Å. This hopping distance is very narrow compared with molecularly doped polymers, that is, the overlap may be significant and effective hopping distances are shortened.

Hole-carrier mobility can be described by the experimental equations (3)–(5) as a function of electric field and temperature followed by Poole–Frenkel and Arrhenius formulations,[12,13]

$$\mu(E,T) = \mu_0 \cdot \exp[-(E_0 - \beta \cdot E^{1/2})/k \cdot T_{\text{eff}}], \tag{3}$$

$$\Delta = E_0 - \beta \cdot E^{1/2}, \tag{4}$$

$$T_{\text{eff}}^{-1} = T^{-1} - T_0^{-1}, \tag{5}$$

where μ_0 is the mobility at a critical temperature (T_0) at which the field dependence of the mobility disappears, E_0 is the activation energy at zero electric field which suggests the depth of the traps, β is the Poole–Frenkel coefficient, which is obtained from the slope of the effective activation $E_0 - \beta \cdot E^{1/2}$ against $E^{1/2}$, E is the electric field, k is Boltzmann's constant, T_{eff} is the effective temperature which is related to the T_0, and Δ is the activation energy. Figure 9 shows the pulse shapes at various temperatures at 10^4 V/cm. Within this temperature region, a large difference cannot be seen. Since the DEAB molecules possess well-overlapped π-electrons states, the small temperature dependence can be observed in this study. Above 305.5 K, the pulse shape is nearly rectangular with well-defined t_T; whereas, below 297.5 K it is too difficult to determine the t_T. This phenomenon indicates a widespread hole packet as it arrives at the substrate electrode. Figure 10 shows the hole mobilities against $\beta \cdot E^{1/2}$ with different temperature from 285 to 335 K. The slopes of the plots are temperature dependent and increased with decreasing temperature.

The Arrhenius plot of the temperature dependence of the mobility, which is expressed by Gill,[10] is plotted in Fig. 11. The field dependence becomes steeper as the temperature is lowered. The activation energy becomes lower in the higher temperature region. From the slope and intercept of the $\log \mu$ vs T^{-1} plot in Figs. 11 and 12, the values were determined as

$$\mu_0 = 8.0 \times 10^{-3} \ (\text{cm}^2/\text{V} \cdot \text{s})$$

$$T_0 = 339 \ (\text{K})$$

$$E_0 = 0.79 \ (\text{eV})$$

$$\beta = 2.12 \times 10^{-3} \ (\text{eV} \cdot \text{cm}^{1/2}/\text{V}^{1/2})$$

$$T_{\text{eff}} = 1.79 \times 10^3 \ (\text{K}).$$

As shown in Fig. 12, the plot of activation energies for each $E^{1/2}$ gives a zero-field activation energy of $E_0 = 0.79$ eV. In general, the field and temperature dependences of the hole mobility below T_g were confirmed to be analyzable by Gill's expression.[10] The T_0 presented here is very close to T_g measured by DSC analysis. The relationship between T_0 and T_g implies that the polymorphic state and dielectric relaxation of the DEAB derivative are important in hopping transport. T_0 has a close connection with T_g, and μ_0 shows the mobility in the liquid state at T_0. Thus, the

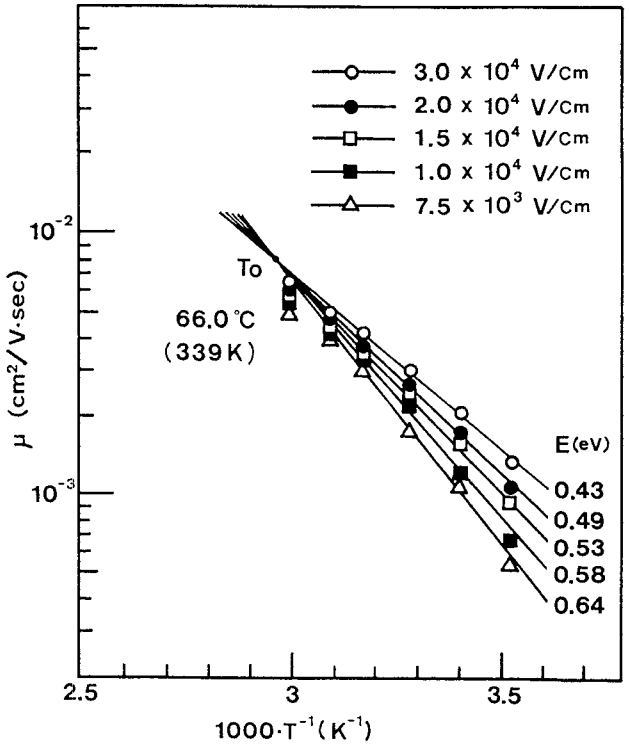

FIG. 11. Arrhenius plot of the hole mobility of DEAB film at different electric field.

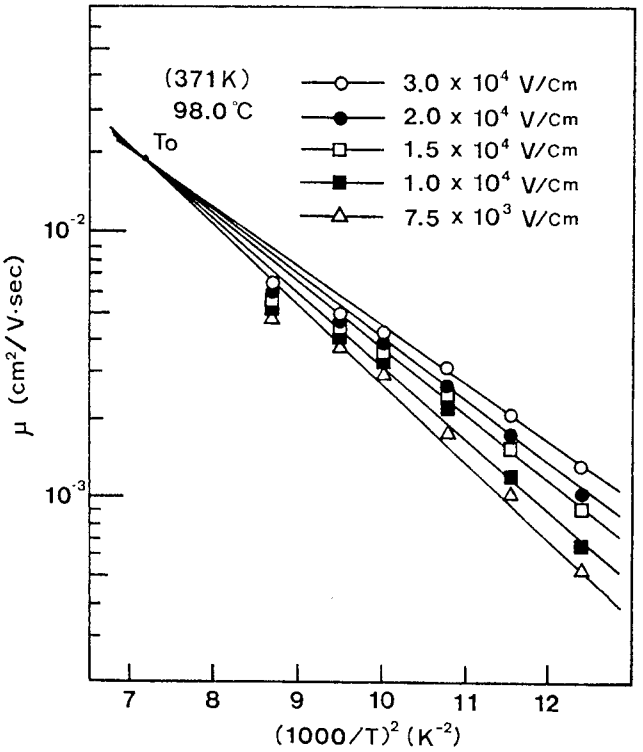

FIG. 13. Log μ vs $(1/T)^2$ dependence of DEAB film at different electric field.

carrier transport in a glassy state was controlled by detrapping of the Poole–Frenkel type in the temperature region under T_0. In the case of this DEAB amorphous film, the temperature dependences of mobility were well-fitted to the Arrhenius type.

F. Temperature dependence of hole mobility followed by Gaussian distribution

The computer simulations of a Gaussian distribution of hopping sites in a trap-free molecular system indicated that the hopping energies were subject to a Gaussian distribution,[13,14] in which the mean activation energy is zero:

$$\mu(T)=\mu_0\cdot\exp[(T_0/T)^2], \tag{6}$$

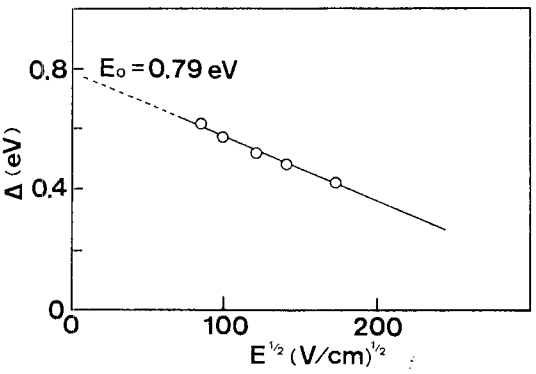

FIG. 12. Activation energy of the mobility vs the square root of applied field.

where T_0 is a characteristic temperature relating to the energy distribution σ of the hopping sites, and μ_0 is the mobility which would be measured if $\sigma/kT\ll 1$, i.e., as $T\to\infty$, and T_0 is obtained from the intersection of the slope measured at various electric fields. The Gaussian width σ of the hopping sites is evaluated from T_0, and $K=T_0/\sigma=7400$ K/eV.[14] From the log μ vs T^{-2} plot in Fig. 13, the values were determined as

$$\mu_0=1.75\times10^{-2}\ (\mathrm{cm^2/V\cdot s}),$$

$$T_0=371\ (\mathrm{K}),$$

$$\sigma=0.050\ (\mathrm{eV}).$$

The Gaussian distribution mechanism can be explained as follows, thus the sheet of holes thermalizes in a Gaussian distribution of states where the distribution is a disorder energy,[6] which is the average of site-to-site potential fluctuation. The μ_0 value of a pure molecular crystal is approximately 1 $\mathrm{cm^2/V\cdot s}$.[15] In the case of an organic amorphous film, the μ_0 value would be decreased due to reduced wave-function overlap. Many researchers have reported μ_0 values between 10^{-3} and 10^{-2} $\mathrm{cm^2/V\cdot s}$.[6,7] The μ_0 value of 1.75×10^{-2} $\mathrm{cm^2/V\cdot s}$ in this study, which suggests the mobility of a disorder-free state, is in agreement with physical interpretations. σ describes the degree of energetic disorder. Bässler shows that a trend exists between σ and the Hammett constant in substituted triphenyl methanes (TPMs), where the substituents are $-N(C_2H_5)_2$, —H, $-OCH_3$, —Br, —CN or $-NO_2$, embedded in bisphenol-*A*-polycarbonate.[7] Both T_0 and σ increase in this

order, on the contrary, the hole mobility decreases in this order. Therefore photoconductive materials containing substitute groups of electron donor are effective in having high hole mobility. The DEAB derivative has two $-N(C_2H_5)_2$ substituent groups, and large π-orbital resonances in a molecule, which will aid smooth hole-carrier transport. The σ values from 0.07 to 0.16 eV were observed, and depended on the substituent and the dopant concentrations.[6,7] Since no insulated polymer was used in this system, the values of T_0 and σ were low compared with other reports.[4–8] However, these values support the high hole mobility of this DEAB amorphous film.

IV. CONCLUSIONS

DSC, XRD patterns, IR spectra, and fluorescence spectra were used for the morphologic study on film and crystal powders of a DEAB derivative. The DSC result of the film of the DEAB derivative indicates the glass transition (T_g; 337.0 K), crystallization (T_c; 385.8 K), and melting temperatures (T_m; 441.0 K). As a result of XRD and annealing, this film shows an amorphous state under the temperature of T_c, although the film over T_c suggests a crystal state, which has the same positions of the XRD lines for the DEAB crystal powder before dissolution for fabrication of the amorphous film. The IR spectrum also supported the increase in the degree of freedom for DEAB molecules in a film. For the amorphous DEAB film, the absorption lines assigned to the out-of-plane C—H bending vibrations of the peripheral benzene rings were not split into two lines.

A hole mobility of the DEAB film in excess of 10^{-3} $cm^2/V\cdot s$ was observed at room temperature. The $E^{1/2}$ dependence of the mobility exhibited a linear relationship with a small field dependence, which suggested relative freedom from deep structural traps. From the analysis of the Poole–Frenkel and Arrhenius formulations, $\mu_0 = 8.0\times10^{-3}$ $cm^2/V\cdot s$, $T_0 = 339$ K, $E_0 = 0.79$ eV, $\beta = 2.12\times10^{-3}$ $eV\cdot cm^{1/2}/V^{1/2}$, $T_{\text{eff}} = 1.79\times10^3$ K could be determined from the well-fitted electric field and temperature dependences of the hole mobilities. The temperature dependence of hole mobility followed by Gaussian distribution was also discussed resulting from the $\log\mu$ vs T^{-2} plots at various electric fields and determined as $\mu_0 = 1.75\times10^{-2}$ $cm^2/V\cdot s$, $T_0 = 371$ K, $\sigma = 0.050$ eV. These values supported the result of the hole mobility on DEAB film. In this study, we could not distinguish whether Arrhenius or non-Arrhenius was a better fit, although we could slightly admit the good fit for temperature dependences in the Arrhenius type of the hole mobility.

ACKNOWLEDGMENT

The authors would like to thank Toyo Ink Mfg. Co., Ltd. for their assistance.

[1] H. Scher and F. W. Montroll, Phys. Rev. B **12**, 2455 (1975).
[2] G. Pfister, Phys. Rev. B **16**, 3676 (1977).
[3] P. M. Borsenberger, W. Mey, and A. Chowdry, J. Appl. Phys. **49**, 273 (1978).
[4] M. Stolka, J. F. Yanus, D. M. Pai, J. Phys. Chem. **88**, 4707 (1984).
[5] L. B. Schein, A. Rosenberg, and S. L. Rice, J. Appl. Phys. **60**, 4287 (1986).
[6] H. Bässler, G. Schonherr, M. Abkowitz, and D. M. Pai, Phys. Rev. B **26**, 3105 (1982).
[7] H. Bässler, Philos. Mag. B **50**, 347 (1984).
[8] H. Ueda, Japan Koho Patent No. 30255 (1987).
[9] T. Hagiwara, U. S. Pat. 4,751, 163 (1988).
[10] W. D. Gill, J. Appl. Phys. **43**, 5033 (1972).
[11] J. Mort and G. Pfister, *Electronic Properties of Polymers* (Wiley & Sons, New York, 1982).
[12] J. X. Mack, L. B. Schein, and A. Peled, Phys. Rev. B **39**, 7500 (1989).
[13] G. Schonherr, H. Bässler, and M. Silver, Philos. Mag. B **44**, 369 (1981).
[14] M. Grunewald, B. Pohlmann, B. Movaghar, and D. Wurtz, Philos. Mag. B **50**, 341 (1984).
[15] L. B. Schein and D. W. Brown, Mol. Cryst. Liq. Cryst. **87**, 1 (1982).